Effect of the Disulfide Bond on the Monomeric Structure of Human Amylin Studied by Combined Hamiltonian and Temperature Replica Exchange Molecular Dynamics Simulations

Rozita Laghaei and Normand Mousseau*

Département de Physique and Regroupement québécois sur les matériaux de pointe, Université de Montréal, C.P. 6128, succursale Centre-ville, Montréal (Québec), Canada

Guanghong Wei

Department of Physics and Surface Physics Laboratory (National Key Laboratory), Fudan University, 220 Handan Road, Shanghai 200433, China

Received: January 8, 2010; Revised Manuscript Received: March 18, 2010

The human Islet amyloid polypeptide (hIAPP or amylin) is a 37-residue peptide hormone that is normally cosecreted with insulin by the pancreatic β-cells. In patients with type 2 diabetes, hIAPP deposits as amyloid fibrils in the extracellular spaces of the pancreatic islets. Recent experimental studies show that the intramolecular disulfide bond between Cys2 and Cys7 plays a central role in the process of fibril formation. However, the effect of the disulfide bond on the intrinsic structural properties of monomeric hIAPP is yet to be determined. In this study, we characterize the atomic structure and the thermodynamics of full-length hIAPP in the presence and absence of a disulfide bond using extensive combined Hamiltonian and temperature replica exchange molecular dynamics simulations (HT-REMD) with a coarse grained protein force field. Our simulations show that HT-REMD is more efficient in sampling than temperature REMD. On the basis of a total simulation time of 28 μs, we find that, although native hIAPP (in the presence of a disulfide bond) essentially adopts a disordered conformation in solution, consistent with the signal measured by ultraviolet-circular dichroism (UV-CD) spectroscopy, it also transiently samples α-helical structure for residues 5−16. In comparison with the N-terminal region, the C-terminal region is highly disordered and populates a much lesser content of isolated β-strand conformation for residues 22−26 and 30−35. Moreover, the absence of the disulfide bond greatly decreases the extent of helix formed throughout residues 5−9 in favor of random coil and β-sheet structure. Implications of the stabilization of N-terminal helical structure by disulfide bond on the initialization of hIAPP amyloid formation are discussed.

I. Introduction

Human islet amyloid polypeptide (hIAPP, also known as amylin) is a 37-residue peptide cosecreted with insulin and produced by β-cells in the pancreas. hIAPP aggregation has been implicated in the loss of β-cell mass, leading to a reduction in insulin production.[1] The hIAPP amyloid deposits, which are found in more than 95% of type-II diabetes patients, are thought to be responsible for the type-II diabetes mellitus. In spite of extensive research,[2–8] the exact toxic mechanism is still unknown and numerous efforts are underway to try to understand the aggregation pathway.[9–14] Under physiological conditions, hIAPP remains soluble and unstructured.[3,15] It contains a disulfide bond between Cys2 and Cys7 and is C-terminally amidated.[16] Both the disulfide bond and the terminal amidation are required for full-length hIAPP hormonal activity, and recent experimental studies suggest that the presence of an intramolecular disulfide bond between Cys2 and Cys7 enhances the hIAPP fiber formation.[17,18] However, the effect of the disulfide bond on the intrinsic structural properties of monomeric hIAPP remains unclear. Meanwhile, due to its high rate of aggregation under the concentration conditions needed for solution NMR, the three-dimensional structure determination of hIAPP monomer under physiological conditions is very challenging.[8] As a result, the tertiary structure of hIAPP peptide in solution is not known. The determination of its monomeric conformations, that could give insights into the intrinsic structural properties relevant to amyloid formation, is therefore even more critical.

Because of the inherent difficulties associated with investigating the structure of hIAPP peptide in aqueous solution under physiological conditions, efforts geared at characterizing its monomeric structure have thus far been limited to secondary structure studies using ultraviolet-circular dichroism (UV-CD) spectroscopy[3,15,19] and NMR studies performed at low pH and low temperature.[9] UV-CD spectroscopic studies show that the peptide adopts an unstructured conformation.[3,15,19] However, it also assumes compact structures as detected by FRET.[20] 2D NMR spectroscopy shows that the monomeric form of hIAPP transiently samples α-helical conformations,[9] in agreement with triplet quenching experiments[21] that reveal a partially structured state of hIAPP monomer in solution. Pulsed-field gradient NMR data also indicate that hIAPP monomer adopts a temperature-dependent compact folded conformation and the compact form of hIAPP monomer might be linked to its later aggregation.[22] Recently, by combining ion mobility mass spectroscopy and all-atom implicit-solvent REMD simulations (200 ns), Dupuis et al.[23] suggested that hIAPP dehydrated solution structures form extended β-hairpins and helix−coil conformations as dehydrated

* To whom correspondence should be addressed. E-mail: normand.mousseau@umontreal.ca.

10.1021/jp100205w
Published on Web 04/29/2010

solution structures of hIAPP. At the moment, however, a detailed characterization of the structures adopted by hIAPP monomer under physiological solution conditions has yet to emerge from experimental studies.

We focus here on the full-length IAPP monomer and, in particular, the role of the disulfide bond on its soluble structure, as there is strong evidence that the presence of the α-helical N-terminal region of IAPP is an important transient stage in the formation of oligomer.[24–26] Comparing the insertion in membranes of full-length rat-IAPP and h-IAPP with h-IAPP$_{1-19}$ and h-IAPP$_{20-29}$, it is found that both h-IAPP and rat-IAPP insert more efficiently than the fragments, with the amyloidogenic fragment (residues 20−29) doing the worst. It seems therefore that the amyloidogenic region of the h-IAPP is available for the fibrillation while the N-terminal residues which are not part of the fibril[27] ease the insertion into the membrane.[28] The role of the α-helical region is also consistent with observations that, contrary to the monomer, the aggregated form of h-IAPP does not have the ability to insert into phospholipidic monolayers;[28] membrane damage would therefore be caused by the monomeric species.[22]

In this context, the role of the disulfide bridge between residues 2 and 7 is unusual. Miranker and his co-worker[17] using optical and mass spectroscopy on truncated IAPP(8−37) and full-length IAPP with and without the disulfide bridge showed that the disulfide bridge between residues 2 and 7 prevents the N-terminal region from the β-strand. Contrary to what could be expected, this restriction seems to help control the assembly mechanism that plays an important role in the fibril formation mechanism. This led Miranker et al. to propose a two-step seeded kinetics where the absence of the disulfide bond eliminates the activation phase of the IAPP polymerization.

To characterize the monomeric structure of hIAPP, especially the impact of the disulfide bridge on its conformations, we carry out replica exchange molecular dynamics simulations (REMD)[29] on hIAPP peptide in the presence and absence of a disulfide bond. Because fully sampling the configurational space of a 37-residue peptide at the all-atom level remains a challenge, simulations are performed using a coarse-grained protein force field, the optimized potential for efficient peptide structure prediction (OPEP).[30] OPEP is coupled here with a modified version of the REMD method, a combined Hamiltonian and temperature REMD (HT-REMD), that accelerates sampling noticeably. This allows us to fully converge thermodynamical sampling and provide a clear description of the monomeric structure of hIAPP and of the structural role of the Cys2−Cys7 disulfide bond.

II. Methods

We investigate the monomeric structures and the thermodynamics of full-length hIAPP (with amino acid sequence KCNTATCATQRLANFLVHSSNNFGAILSSTNVGSNTY) in two different forms, the C-amidated form of hIAPP with a disulfide bridge between residues Cys2 an Cys7 (wild-type, named WT-hIAPP) and its disulfide broken-bond variant (reduced form, named R-hIAPP). The intra- and interpeptide interactions are described using OPEP version 3.2.[30] OPEP represents the amino acids by all of the heavy backbone atoms, Cα, N, C, O, as well as the amine hydrogen H. It uses a single bead to represent the side chains of the amino acids. OPEP's parameters, which are fitted to include the effect of solvent implicitly, are described in details in refs 30 and 31. Although the properties of peptides using the implicit solvent model have not been tested as widely as for explicit-solvent models, OPEP version 3.2 has been shown to differentiate between the native and non-native form of a large set of proteins and peptides.[30] Moreover, OPEP, combined with the activation−relaxation technique, was able to identify generic peptide aggregation mechanisms such as the reptation of the chains[32] that were confirmed experimentally[33] and theoretically with more sophisticated force fields.[34] OPEP was also shown to recover the experimental structural and thermodynamical properties of several peptides starting from random states[12,35–37] and the free energy surface of the all-atom Aβ_{16-22} dimer in explicit solvent[38] using MD (or T-REMD) simulations.

OPEP is used here with combined HT-REMD. Standard T-REMD involves the parallel simulation of N replicas of a system at N different temperatures. At regular time intervals, replica i is exchanged with its neighbor j with a probability given by

$$p(i,j) = \min\left\{1.0, \exp\left[\left(\frac{1}{k_B T_i} - \frac{1}{k_B T_j}\right)(E_i - E_j)\right]\right\} \quad (1)$$

where E_i is the configurational energy of replica i and T_i, the initial temperature of the same replica.

Formally, REMD is not confined to sampling along the temperature axis and numerous other parameters, such as the hydrophobic interaction strength,[39] have been used. Here, we introduce a combination of Hamiltonian and temperature REMD, which mixes temperature and interaction strength in order to facilitate configurational sampling for dense polymers, such as large proteins and aggregates. These systems are dominated by states with much lower entropy than others and for which simply increasing temperature in REMD does not significantly help the reversible exploration of folding pathways.[40] To overcome this limitation, we propose the following procedure: (i) a set of $N - M$ replicas are run at $N - M$ different temperatures with exchanges following eq 1; (ii) M replicas are also run at the highest temperature but with variable interaction strength. These are exchanged according to

$$p(i,j) = \min\{1.0, \exp[-\beta([H_i(X') + H_j(X)] - [H_i(X) + H_j(X')])]\} \quad (2)$$

where $H_i(X')$ is the Hamiltonian of configuration X' for replica i and configurations X and X' are the configurations for replicas i and j, respectively.

While in standard REMD complex conformations hardly explore the configurational space even at high temperature, in combined HT-REMD, the high-temperature low-attraction configurations can reorganize themselves easily into new states that retain a reasonable probability of being accepted and propagated to lower temperature. As we show in the Discussion section, the efficiency gain of HT-REMD over T-REMD for a simple system such as monomeric IAPP is about a factor of 3, small but non-negligible. Moreover, it should improve significantly for oligomers and longer chains.

HT-REMD simulations are carried out for both the wild-type and the reduced (disulfide-broken) full-length hIAPP starting from a random conformation generated in short high temperature MD runs, while T-REMD is run for comparison for WT-hIAPP only. Forty replicas are used in all cases, running for 700 ns per replica, resulting in a cumulative simulation time of 28 μs for each REMD run. In the T-REMD simulation, temperatures range from 240 to 700 K. In HT-REMD runs, 35 temperatures range from 240 to 555 K and the remaining five replicas are

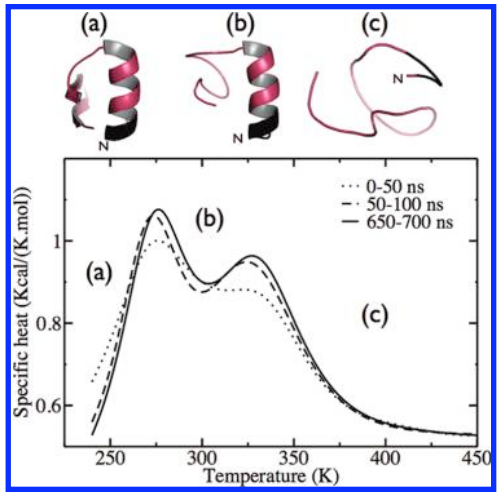

Figure 1. Specific heat curves as a function of temperature at three time intervals for WT-IAPP using the HT-REMD method. Representative structures in the three regions labeled as (a)−(c) in the specific heat plot are shown at the top of this figure. Residues 5−16 form the α-helix in (a) and (b).

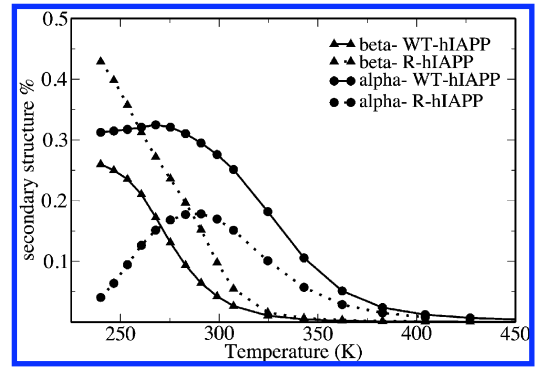

Figure 2. Evolution of α and β contents as a function of temperature for WT-hIAPP (solid line) and R-hIAPP (dotted line) using HT-REMD. Triangles are for β-strand and circles for α-helix.

run at 555 K with a varying scaling on the attractive terms of the interactions—nonbonded and hydrogen bonding—set at 0.8, 0.7, 0.6, 0.4, and 0.2 of the full-strength terms. To choose the right scaling parameters, we select four or five scaling values between 0 and 1 and test the system in a short simulation time to optimize the exchange rate between the scaled and the temperature replicas, making sure that the chains can move freely and separate (disaggregate) from each other when the attraction potential is reduced.

The monomers are placed in a 60 Å-radius confining sphere with reflecting boundary conditions, and the temperature is set with an external bath with a coupling time of 500 fs.[41] A 1.5 fs time-step is used for all three sets of the simulations. Exchanges are attempted every 15 ps, and the RATTLE algorithm is used to constrain the bond length of the peptides.[42]

Except for the convergence check (Figures 1 and 8), all quantities presented here are averaged over the last 200 ns of the 700 ns simulation, which represents a total of 26 600 conformations.

We use the weighted histogram method adapted to replica exchange (PTWHAM) for the thermodynamical analysis.[43] The STRIDE program[44] is used to obtain secondary structure percentages. Side chains are considered in contact if they are less than 6.5 Å apart. Clustering analysis is carried out iteratively as reported in a previous study[45] using a C_α root-mean-square deviation (rmsd) cutoff of 2.25 Å. The structure with the largest number of neighbors deviating by less than 2.25 Å C_α-rmsd was taken, together with the neighbors, to form the first cluster and eliminated from the pool of structures. This process was repeated until there was no structure left in the pool.

III. Results

We focus here on the HT-REMD results for the wild-type hIAPP and the reduced hIAPP. We will present a comparison with T-REMD for WT-hIAPP in the last part of this section, showing that the results obtained from the two techniques are consistent with each other and that HT-REMD reaches thermodynamical convergence significantly faster.

A. Thermodynamics and Structure of hIAPP with a Disulfide Bridge. HT-REMD simulations on the WT-hIAPP monomer are performed following the prescription described in the Methods section, starting from a random conformation generated in a short high-temperature MD simulation.

Before discussing the results, it is necessary to establish that the system is equilibrated. For this, we probe the evolution of the heat capacity in time intervals of 50 ns. Because heat capacity is dominated by the presence of low-energy stable structures, it is very sensitive to the sampling quality of the algorithm. Figure 1 shows this evolution for the WT-hIAPP. We see that C_V converges within the first 50 ns, as the specific heat curve for the 50−100 ns interval is similar to the one for the last 50 ns of the 700 ns simulation. For comparison with T-REMD, which converges more slowly (as shown in the next section), however, we use only data generated in the last 200 ns of the simulation for various analyses. The results are unchanged if we use a larger data set.

The converged heat capacity shows two peaks with the structures given above the curve representing the centers of the largest cluster in each region of the graph. At low temperature (below 278 K), WT-hIAPP monomer in the first populated cluster adopts a well-defined structure with an α-helix at residues 5−16 and a β-hairpin with two β-strands at residues 22−27 and 30−36 positioned in a perpendicular orientation with respect to the α-helix (structure (a) at the top of Figure 1). The first peak at 278 K is caused by the unfolding of the β-hairpin, while the α-helix remains intact. As is shown by structure (b), the C-terminal remains close to the conformations adopted at lower temperature and helps to stabilize the helix. The second peak at 322 K is associated with the total destabilization of the peptide's secondary structure. While the helix can still be observed near the peak, it is generally shorter and short-lived (not shown), with a very flexible C-terminal. Most of the time, however, the peptide is unstructured, similar to structure (c) in Figure 1. This smooth unfolding process can be seen more clearly in Figure 2 which shows the average secondary structure as a function of temperature. In particular, we see that the β-sheet content decreases rapidly with temperature to less than 5% at 300 K, while the proportion of α-helices remains constant (and even increases slightly) at 30% up to 290 K, before decreasing slowly to vanish near 400 K. The stability of the α-helix over a wide range of temperatures is in agreement with experimental data by ref 22 which studies the structural changes for rat IAPP and hIAPP by temperature (from 277 to 310 K) using pulsed-field gradient NMR and circular dichroism spectroscopy.

After this characterization of the temperature dependence of WT-hIAPP, we now focus on its structural features at room temperature. The secondary structure propensity for each residue at 300 K is plotted in Figure 3 and shows that the partially

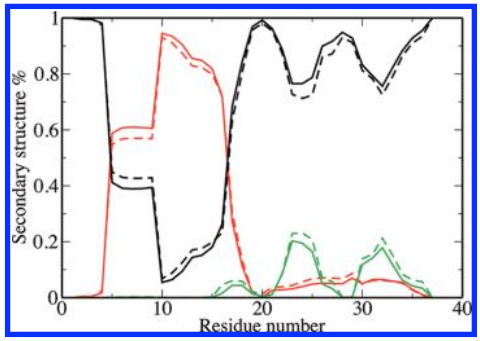

Figure 3. Percentage of secondary structures as a function of residue number for WT-hIAPP at 300 K. The results shown by solid lines and broken lines are obtained by HT-REMD and T-REMD, respectively. Green, β-sheet; red, α-helix; black, coil+turn.

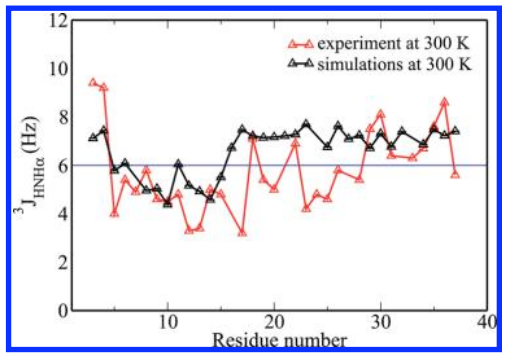

Figure 4. $^3J_{HNH\alpha}$ calculated for WT-hIAPP at 300 K for residues 3−37 using the data generated in our HT-REMD run. For comparison, the experimental data for hAIPP bound to SDS micelle is also shown (red).[25] The error bars are smaller than the figure symbols.

disordered peptide has some well-defined secondary structures. As observed above, residues 5−16 form a relatively stable helix. The helical propensity of these residues varies between 60 and 90%, as shown in Figure 3. Much rarer, with a propensity between 10 and 20%, a β-sheet spanning residues 22−27 and 30−35 is still visited, extending, with an even smaller probability, to a third β-sheet at residues 16−19 when the α-helix is destabilized. The high propensity for the N-terminal residues 5−16 to adopt a helical structure is consistent with NMR spectroscopic results at room temperature.[18]

To provide quantitative data for comparison with experiments, we compute the $^3J_{HNH\alpha}$ coupling[46,47] for hIAPP at 300 K. This quantity is used to characterize the HNH_α angle associated with the ϕ dihedral angles. Our calculated sequence profile for $^3J_{HNH\alpha}$ coupling is shown in Figure 4. As a measure of dihedral angles, a coupling below 6 Hz indicates that the local environment is in ϕ dihedral angle range associated with an α-helix. It can be seen in Figure 4 that the *J*-couplings of residues 5−15 are below 6 Hz and those of residues 16−36 are well above, as expected from the discussion above.

Due to the high rate of aggregation for hIAPP in aqueous solution, there are no $^3J_{HNH\alpha}$ couplings obtained from experiment in solution for direct comparison and our calculated couplings will provide useful information for future 3D HNHA experiment for hIAPP in solution. However, experimental *J*-couplings for hIAPP bound to SDS micelle have been reported recently by Patil et al.[25] and it is useful to compare with our simulation even though the two systems are not identifcal. Experimental results indicate that the peptide has a very stable α-helix in the 5−16 region, with a second helix between 22 and 28, separated by a disordered region between residues 18 and 22. The C-terminal region, residues 28−37, is disordered.[25] Our results

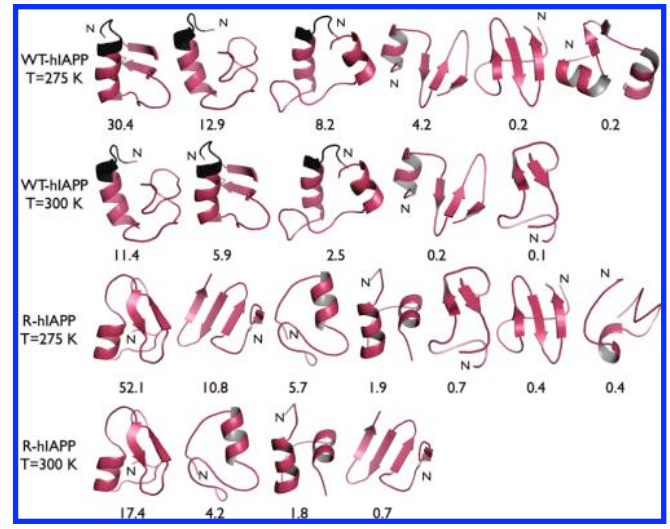

Figure 5. Center of the main structural classes and their respective probability for WT-hIAPP at (a) 275 K and (b) 300 K and for R-hIAPP at (c) 275 K and (d) 300 K. Classes are obtained as described in the text.

are in agreement with the experiments in the N-terminal 5−15 and the C-terminal 29−37 regions. The main discrepancy is in the 17−28 region, where we tend to observe random coil or β-sheet structure even though an α-helix can form, with very small probability (Figure 3). This can be explained by the presence of the micelle, that prevents the C-terminal from folding over the peptide, as we observe in Figure 1, favoring a more extended structure, compatible with α-helical conformations and in agreement with the observation by Patil et al. that this second helix (22−28) is less stable than the first one.[25] The additional stabilization provided by the micelle can also explain the higher stability of the N-terminal helix observed in the experiment as compared with the simulation presented here.

To characterize the three-dimensional structures of WT-IAPP, cluster analysis is performed over the 26 600 conformations of the last 200 ns of the simulation. Using a C_α-rmsd cutoff of 2.25 Å, the center of the first 100 largest clusters are obtained and then regrouped, using a visual assessment of the overall shape and secondary structure, into structural classes. These structural classes, sampled at 275 and 300 K and representing, respectively, 56 and 20% of all structures, are shown in Figure 5. At 275 K, the α-helical structure dominates in the N-terminal region, often stabilized by a perpendicular structure that can be either a β-sheet, a small α-helix, or even a random-coil conformation. We recover the small dominant structures at 300 K, although in a different order and with lower probability: the WT-hIAPP monomer primarily adopts partially unstructured conformations. Nevertheless, in the three dominant classes at both temperatures, the helical structure spans a continuous stretch over 40% of the peptide from residues 5−19 (Figure 3).

B. Thermodynamics and Structure of hIAPP without a Disulfide Bridge. HT-REMD simulations are also carried out on the reduced form of hIAPP. The thermodynamical and structural properties of R-hIAPP are investigated following the same approach as for WT-IAPP, and for ease of comparison, only the last 200 ns of a 700 ns HT-REMD simulation are used in the analysis. The specific heat as a function of temperature is presented in Figure 6. It shows a rather different curve from that of WT-hIAPP, with a small shoulder at 265 K and a significant peak at 299 K. As can be seen from the structures represented above the curve, the shoulder corresponds to the

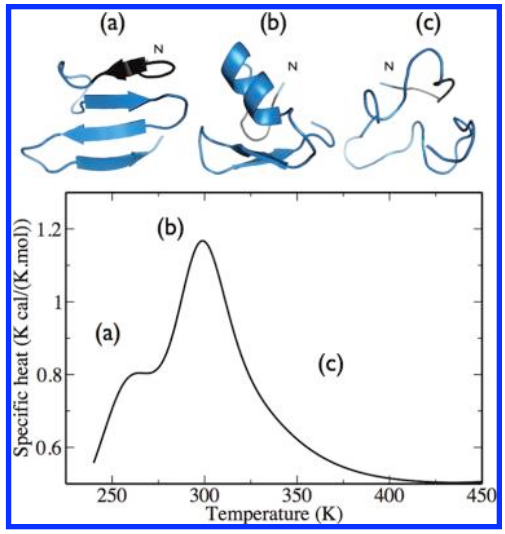

Figure 6. Specific heat for R-hIAPP as a function of temperature T, obtained from HT-REMD simulation. Representative structures in the three regions labeled as (a)−(c) in the specific heat plot are shown at the top of this figure.

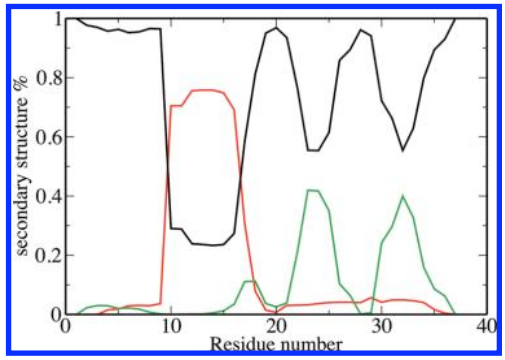

Figure 7. Secondary structure probability as a function of residue number for R-hIAPP. Green, β-content; red, α-helix content; black, coil+turn contents.

transformation of the N-terminal β hairpin, part of a four β-strand structure (Figure 6a), into an α-helix (Figure 6b). This transition is relatively mild, energetically speaking, since both the initial and final structures show a similar degree of ordering while the main peak at 299 K is associated with an order−disorder transition (Figure 6c).

The structural evolution of R-hIAPP is captured in Figure 2, which shows the average secondary structure as a function of temperature. The most striking feature is the sharp decrease in β-sheet content, from 45% at 240 K to less than 5% at 310 K, which is accompanied by a considerable growth of the α-helical content, from less than 5% at 240 K to 18% at 295 K, before falling again to less than 5% around 360 K. Comparison with its oxidized counterpart shows that R-hIAPP disfavors the helical conformation at all temperatures.

This is clearly seen in Figure 7, which shows the secondary structure probability for each residue at 300 K. While the N-terminal residues sample helical structure with high probability, the helix is shorter than that of WT-hIAPP, running from residues 10 to 16. The loss of helical structure from residues 5 to 9 results from the absence of a disulfide bond between Cys2 and Cys7 in the R-hIAPP. However, the percentage of β-sheets at residues 22−27 and 30−35 reaches 30% in the absence of the disulfide bridge, much higher than that of WT-hIAPP. Three-dimensional representations of the dominant classes for R-hIAPP, obtained following the same procedure as for its wild type, are given in Figure 5. These structural classes sampled at

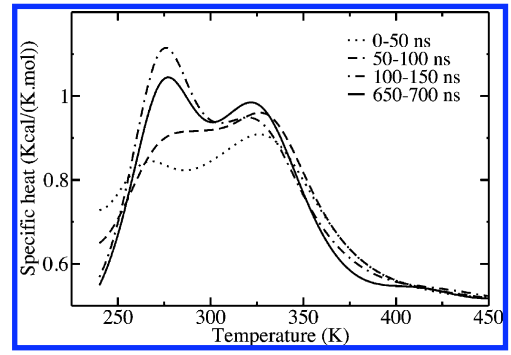

Figure 8. Specific heat curves as a function of temperature at three time intervals for WT-hIAPP using the T-REMD method. Dotted line, 0−50 ns; dashed line, 50−100 ns; dot−dashed line, 100−150 ns; solid line, 650−700 ns.

275 and 300 K represent, respectively, 72 and 24% of all structures. With a respective probability of 52 and 17%, the most populated class of conformations at both 275 and 300 K is a short α-helix, spanning residues 10−16, and making contact with a β-hairpin positioned in a parallel orientation.

At 300 K, the second populated class, with a population of 4%, is a compact state with helical structure at residues 10−16. The conformations in the third classes, with a much lower population of 2%, have helical structures with two short helices involving residues 8−19 and 27−34. A four-stranded β-sheet structure is observed in the fourth classes, with a negligible population (1%). Overall, our results demonstrate that the absence of a disulfide bond in R-hIAPP reduces the content of helix formed through residues 5−9, consistent with the results suggested by NMR spectroscopy for rat IAPP monomer.[48]

C. HT-REMD vs T-REMD. To validate the results obtained from our HT-REMD simulations, we compare with standard 40-replica REMD simulations performed on the wild-type hIAPP with a temperature range from 240 to 700 K for 700 ns of each replica, while HT-REMD is run over 35 temperatures ranging from 240 to 555 K, with an additional five replicas run at 555 K with attractive forces decreasing by a factor 0.8 to 0.2. Higher temperature trajectories are necessary in T-REMD in order to enhance sampling and prevent the peptide from getting trapped in local minima. In HT-REMD, this need is circumvented by a rescaling of the attractive part of the potential. This modification allows us to run at lower temperatures, decreasing the probability of finding configurations with an unfavorable steric environment.

To establish the interest of HT-REMD, we show that this algorithm converges faster than T-REMD to thermodynamical equilibrium. This can be seen by looking at the convergence of the specific heat, reported in Figures 1 and 8, respectively, for HT-REMD and T-REMD. While the Hamiltonian-temperature REMD specific heat converges within 50 ns, it takes more than 150 ns for the standard algorithm to converge, even with a relatively simple system such as the 37-residue IAPP peptide. We note that, once equilibrated, both methods lead to the same sampling statistics, as can be seen in Figure 3, which plots the secondary structure probability for each residue at 300 K, averaged over the last 200 ns of the 700 ns simulations, both for T-REMD (dashed lines) and HT-REMD (solid lines).

While a factor of 3 in sampling efficiency is non-negligible, as sampling configurations become more difficult with larger systems, HT-REMD should provide an even greater efficiency gain over standard REMD. This is especially so in dense systems where the decrease of the attractive force generates a considerably improved sampling of hard to reach conformations.

IV. Discussion

Simulations on the IAPP monomer with and without the Cys2−Cys7 disulfide bridge provide a clear picture for the crucial role played by this covalent bond on the sequence's thermodynamical and structural properties. They show that the identical sequence for the two peptides studied leads to similar structures being visited. However, the single disulfide bridge at the N-terminal is sufficient to differentiate qualitatively the peptide's average properties.

Let us consider first the similarities. These are most obvious when looking at the dominant classes at 275 and 300 K (Figure 5) as well as the secondary structure probability profile computed at 300 K (Figures 3 and 7). While visited with different weight, a number of nontrivial classes are shared by the two peptides. The same three-stranded β-sheet, for example, is found both for WT-hIAPP and for R-hIAPP, albeit with different probability. For WT-hIAPP, this structure exists only at 275 K, and with a probability of 0.2%, while it is found with a probability of 11 and 0.7% at 275 and 300 K, respectively, for R-hIAPP, if we also include the four-stranded β-sheet. Similar α-helical conformations are also found for both sequences although oriented in opposite directions. The third class of WT-hIAPP at 275 and 300 K show antiparallel helices, while R-hIAPP classes number four and three at 275 and 300 K, respectively, show the same helices but in parallel organization.

The main difference between the two peptides is therefore not so much in the allowed conformations but in the thermodynamical weight of these various structural elements, as is observed, for example, in Figure 2, where we see that the β-strand content is much lower and the α-helical probability much higher for the wild-type IAPP than the reduced one. The disulfide bridges stabilize the helix at residues 5−9 on a fragment that would otherwise remain disordered. This forcing generates a domino effect, with the presence of an α-helix at residues 5−9 biasing the helical formation in the following residues, 10−16, as is also clearly seen when looking at the dominant classes, Figure 5. From the same figure, we also see the impact of the disulfide on the overall protein extension. In agreement with recent triplet quenching experiments,[21] we observe that the end-to-end distance is significantly smaller for WT-hIAPP than for R-hIAPP (Figure 9 (top)) at room temperature. However, the proximity of the two end points is caused by the general organization of the protein and not an overall compaction. For example, as mentioned above, the antiparallel two-helix conformations visited by WT-hIAPP directly brings the two end-points together, while the parallel organization favored by R-hIAPP has the opposite effect. In general, as is seen in Figure 9 (bottom), the absence of a disulfide bridge allows the protein to explore significantly more compact structures than for the wild-type.

These numerical results are fully consistent with recent experiments. For example, experimental studies using spectroscopic techniques show that WT-hIAPP under biologically relevant solution conditions sample helical structure across residues 5−19 and the formation of this helical structure is directly correlated with enhanced amyloid formation in solution.[48] This work also shows that the absence of the disulfide bond decreases the extent of helix formed in the N-terminal region and the decrease of helix reduces the rate of hIAPP aggregation.[17]

It is interesting to speculate on the connection between the stabilization of N-terminal helical structure by disulfide bond and the initiation of hIAPP aggregation. Recent NMR spectroscopic data suggest that the N-terminal region of WT-hIAPP (residues 1−17), and not the main amyloidogenic region (residues 20−29) of hIAPP, is involved in the initial self-association of the peptide in bulk solution.[9] Consistent with this experimental study, Abedini and Raleigh proposed that early oligomerization of hIAPP is linked to helix formation and is promoted by helix−helix association.[49] A recent structural analysis of hIAPP by 1H NMR shows that R-hIAPP polymerizes slower than oxidized IAPP.[18] The role of the disulfide bridge in the early steps of hIAPP aggregation has been studied by implicit solvent molecular dynamics simulations.[11] This computational study suggests that hIAPP has a tendency to collapse into amorphous aggregates with less β-sheet content in the presence of the bridge.

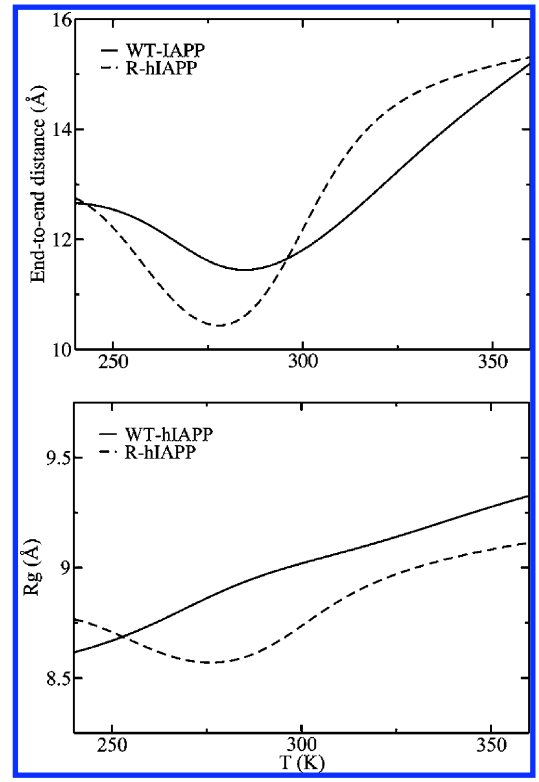

Figure 9. (top) Comparison of the end-to-end distance as a function of temperature for WT-hIAPP and R-hIAPP. (bottom) Comparison of the radius of gyration for the same time interval.

V. Conclusions

We studied the thermodynamic and structural properties of the full-length hIAPP with a disulfide bridge and the disulfide broken bond using HT-REMD with a coarse grained forcefield. Our HT-REMD simulations on the reduced and oxidized forms of hIAPP demonstrate that the disulfide bond stabilizes the helical structures spanning residues 5−19. Experiments together with our simulations suggest therefore that the disulfide bridge is present to stabilize the N-terminal helical structure and facilitate the initialization of hIAPP aggregation encoded at the monomeric level.

Acknowledgment. N.M. acknowledges support from the Natural Sciences and Engineering Research Council of Canada and the Canada Research Chair Foundation. G.W. acknowledges the financial support from the program of New Century Excellent Talent in University (NCET-08-0125). Calculations were done on the computers of the *Réseau québécois de calcul de haute performance*.

References and Notes

(1) Höppener, J. W.; Lips, C. J. *Int. J. Biochem. Cell Biol.* **2006**, *38*, 726–736.

(2) Mirzabekov, T. A.; Lin, M. C.; Kagan, B. L. *J. Biol. Chem.* **1996**, *271*, 1988–1992.

(3) Kayed, R.; Bernhagen, J.; Greenfield, N.; Sweimeh, K.; Brunner, H.; Voelter, W.; Kapurniotu, A. *J. Mol. Biol.* **1999**, *287*, 781–796.

(4) Luca, S.; Yan, W.-M.; Leapman, R.; Tycko, R. *Biochemistry* **2007**, *46*, 13505–13522.

(5) Wilzius, J. J.; Sievers, S. A.; Sawaya, M. R.; Cascio, D.; Popov, D.; Riekel, C.; Eisenberg, D. *Protein Sci.* **2008**, *18*, 1467–1474.

(6) Brender, J. R.; Lee, E. L.; Cavitt, M. A.; Gafni, A.; Steel, D. G.; Ramamoorthy, A. *J. Am. Chem. Soc.* **2008**, *130*, 6424–6429.

(7) Engel, M. F. M.; Khemtemourian, L.; Kleijer, C. C.; Meeldijk, H. J. D.; Jacobs, J.; Verkleij, A. J.; de Kruijff, B.; Killian, J. A.; Hoeppener, J. W. M. *Proc. Natl. Acad. Sci. U.S.A.* **2008**, *105*, 6033–6038.

(8) Engel, M. F. *Chem. Phys. Lipids* **2009**, *160*, 1–10.

(9) Mishra, R.; Geyer, M.; Winter, R. *ChemBioChem* **2009**, *10*, 1769–1772.

(10) Jiang, P.; Xu, W.; Mu, Y. *PLoS Comput. Biol.* **2009**, *5*, e1000357.

(11) Milardi, D.; Pappalardo, M.; Pannuzzo, M.; Grasso, D. M.; Rosa, C. L. *Chem. Phys. Lett.* **2008**, *463*, 396–399.

(12) Mo, Y.; Lu, Y.; Wei, G.; Derreumaux, P. *J. Chem. Phys.* **2009**, *130*, 125101-1–125101-6.

(13) Friedman, R.; Pellarin, R.; Caflisch, A. *J. Mol. Biol.* **2009**, *387*, 407–415.

(14) Takeda, T.; Klimov, D. K. *Biophys. J.* **2009**, *96*, 442–452.

(15) Higham, C. E.; Jaikaran, E. T.; Fraser, P. E.; Gross, M.; Clark, A. *FEBS Lett.* **2000**, *470*, 55–60.

(16) Clark, A.; Lewis, C. E.; Willis, A. C.; Cooper, G. J. S.; Morris, J. F.; Reid, K. B. M.; Turner, R. C. *Lancet* **1987**, *330*, 231–234.

(17) Koo, B. W.; Miranker, A. D. *Protein Sci.* **2005**, *14*, 231–239.

(18) Yonemoto, I. T.; Kroon, G. J. A.; Dyson, H. J.; Balch, W. E.; Kelly, J. W. *Biochemistry* **2008**, *47*, 9900–9910.

(19) Goldsbury, C.; Goldie, K.; Pellaud, J.; Seelig, J.; Frey, P.; Kistler, S. A. M. J.; Cooper, G. J. S.; Aebi, U. *J. Struct. Biol.* **2000**, *130*, 352–362.

(20) Padrick, S. B.; Miranker, A. D. *J. Mol. Biol.* **2001**, *308*, 783–794.

(21) Vaiana, S. M.; Best, R. B.; Yau, W.-M.; Eaton, W. A.; Hofrichter, J. *Biophys. J.* **2009**, *97*, 2948–2957.

(22) Soong, R.; Brender, J. R.; Macdonald, P. M.; Ramamoorthy, A. *J. Am. Chem. Soc.* **2009**, *131*, 7079–7085.

(23) Dupuis, N. F.; Wu, C.; Shea, J.-E.; Bowers, M. T. *J. Am. Chem. Soc.* **2009**, *131*, 18283–18292.

(24) Apostolidou, M.; Jayasinghe, S. A.; Langen, R. *J. Biol. Chem.* **2008**, *283*, 17205–17210.

(25) Patil, S. M.; Xu, S.; Sheftic, S. R.; Alexandrescu, A. T. *J. Biol. Chem.* **2009**, *284*, 11982–11991.

(26) Nielsen, J. T.; Bjerring, M.; Martin, D. Jeppesen; , R. O. P.; Pedersen, J. M.; Hein, K. L.; Vosegaard, T.; Skrydstrup, T.; Otzen, D. E.; Nielsen, N. C. *Angew. Chem., Int. Ed.* **2009**, *48*, 2118–2121.

(27) Kajava, A. V.; Aebi, U.; Steven, A. C. *J. Mol. Biol.* **2005**, *348*, 247–252.

(28) Engel, M. F.; Yigittop, H.; Elgersma, R. C.; Rijkers, D. T. S.; Liskamp, R. M. J.; de Kruijff, B.; Hoppener, J. W. M.; Killian, J. A. *J. Mol. Biol.* **2006**, *356*, 783–789.

(29) Sugita, Y.; Okamoto, Y. *Chem. Phys. Lett.* **1999**, *314*, 141–151.

(30) Maupetit, J.; Tuffery, P.; Derreumaux, P. *Proteins: Struct., Funct., Bioinf.* **2007**, *69*, 394–408.

(31) Derreumaux, P. *J. Chem. Phys.* **1999**, *111*, 2301–2310.

(32) Santini, S.; Wei, G. H.; Mousseau, N.; Derreumaux, P. *Structure* **2004**, *12*, 1245–1255.

(33) Petty, S. A.; Decatur, S. M. *Proc. Natl. Acad. Sci. U.S.A.* **2005**, *102*, 14272–14277.

(34) Strodel, B.; Whittleston, C. S.; Wales, D. J. *J. Am. Chem. Soc.* **2007**, *129*, 16005–16014.

(35) Lu, Y.; Derreumaux, P.; Guo, Z.; Mousseau, N.; Wei, G. *Proteins* **2009**, *75*, 954–963.

(36) Chebaro, Y.; Dong, X.; Laghaei, R.; Derreumaux, P.; Mousseau, N. *J. Phys. Chem. B* **2009**, *113*, 267–274.

(37) Chebaro, Y.; Mousseau, N.; Derreumaux, P. *J. Phys. Chem. B* **2009**, *113*, 7668–7675.

(38) Wei, G.; Song, W.; Derreumaux, P.; Mousseau, N. *Front. Biosci.* **2008**, *13*, 5681–5692.

(39) Fukunishi, H.; Watanabe, O.; Takada, S. *J. Chem. Phys.* **2002**, *116*, 9058–9067.

(40) Faraldo-Gomez, J. D.; Roux, B. *J. Comput. Chem.* **2007**, *28*, 1634–1647.

(41) Berendsen, H.; Postma, J.; van Gunsteren, W.; Nola, A. D.; Haak, J. *J. Chem. Phys.* **1984**, *81*, 3684–3690.

(42) Andersen, H. C. *J. Comput. Phys.* **1983**, *52*, 26–41.

(43) Chodera, J. D.; Swope, W. C.; Pitera, J. W.; Seok, C.; Dill, K. A. *J. Chem. Theory Comput.* **2007**, *3*, 26–41.

(44) Frishman, D.; Argos, P. *Proteins* **1995**, *23*, 566–579.

(45) Daura, X.; Gademann, K.; Jaun, B.; Seebach, D.; van Gunsteren, W. F.; Mark, A. E. *Angew. Chem., Int. Ed. Engl.* **1999**, *38*, 236–240.

(46) Vuister, G. W.; Bax, A. *J. Am. Chem. Soc.* **1993**, *115*, 7772–7777.

(47) Hu, J.; Bax, A. *J. Am. Chem. Soc.* **1997**, *119*, 6360–6368.

(48) Williamson, J. A.; Loria, J. P.; Miranker, A. D. *J. Mol. Biol.* **2009**, *393*, 383–396.

(49) Abedini, A.; Raleigh, D. P. *Phys. Biol.* **2009**, *6*, 015005.

JP100205W